energies

MDPI

Article

Adjustable Capability Evaluation of Integrated Energy Systems Considering Demand Response and Economic Constraints

Yang Li [1,*], Rongqiang Li [1,*], Linjun Shi [1], Feng Wu [1], Jianhua Zhou [2], Jian Liu [2] and Keman Lin [1]

[1] College of Energy and Electrical Engineering, Hohai University, Nanjing 211100, China; 19990041@hhu.edu.cn (L.S.); wufeng@hhu.edu.cn (F.W.); linkeman@hhu.edu.cn (K.L.)
[2] State Grid Jiangsu Electric Power Company Research Institute, Nanjing 211100, China
* Correspondence: eeliyang@hhu.edu.cn (Y.L.); 221606030022@hhu.edu.cn (R.L.)

Abstract: The coupling between multiple energy sources such as electricity, gas, and heat is strengthened in an integrated energy system (IES), and this, in turn, improves the operational flexibility of the IES. As an upper-level energy supply system, an IES can play a role as virtual energy storage, which can provide regulating power to smooth out the volatility from large-scale renewable energy generation. The establishment of an aggregating virtual energy storage model for IESs has become an important issue. Under this background, a multi-objective optimization-based adjustable capacity evaluation method is proposed in this paper. Firstly, the mathematical model of an IES considering the coupling of multiple kinds of energy forms is proposed. Then, an aggregating model considering demand response and economic constraints is established to demonstrate the adjustable capacity of the IES. In addition, multi-objective optimization is used to identify parameters in the proposed model, and the normal boundary intersection (NBI) method is used to solve the problem. Finally, a simulation example is provided to verify the effectiveness and feasibility of the proposed method. The external energy demand boundary of the IES can be modeled as virtual energy storage, and the coupling relations of electricity and gas can be presented. Case studies demonstrate that economic constraints narrow the adjustable capacity of the IES while the demand response extends it.

Keywords: integrated energy system; adjustable capability; demand response; economic constraints; multi-objective optimization; normal boundary intersection

Citation: Li, Y.; Li, R.; Shi, L.; Wu, F.; Zhou, J.; Liu, J.; Lin, K. Adjustable Capability Evaluation of Integrated Energy Systems Considering Demand Response and Economic Constraints. *Energies* **2023**, *16*, 8048. https://doi.org/10.3390/en16248048

Academic Editor: Mariano Giuseppe Ippolito

Received: 20 November 2023
Revised: 8 December 2023
Accepted: 12 December 2023
Published: 13 December 2023

1. Introduction

In recent years, the energy consumption structure dominated by non-renewable energy has caused serious pollution, causing severe challenges such as environmental and climate change [1,2]. The emergence and development of renewable generations (RGs) provide an opportunity to address such problems [3,4]. An integrated energy system (IES) achieves multi-energy interaction, realizing the stepped utilization of energy by coupling various energy forms such as electricity, gas, and heat, and gives full attention to the complementary characteristics of various heterogeneous energy sources [5,6]. With the coupling of multi-energy forms, the efficiency of energy utilization is improved compared with that of the independent operation of various energy sectors [7,8]. An IES engages with the upper energy supply system (UESS) via the procurement of energy such as electricity and natural gas. Because of the complementary coupling of multi-energy resources in IESs, the energy requirement of an IES for a UESS is no longer a fixed value of a single energy resource but a requirement interval of multi-energy resources. An IES, for the UESS, is an integrated load with adjustable potential, and thus the IES can be guided by the UESS to provide regulating power or participate in demand response by issued incentives [9,10]. From the view of dispatching, the centralized dispatching method that informs the UESS's dispatching operator of various equipment information is difficult to ensure user privacy. At the same time, with the increase in distributed flexible resources, the centralized dispatching mode

places great burdens on communication. In this paper, an IES is aggregated and modeled as virtual energy storage, which can be easily embedded into the existing dispatching architecture. Moreover, it requires that IESs clarify their own adjustable range to participate in market bidding. Therefore, a study on the adjustable capacity of IESs considering various factors is important and necessary.

The adjustable capacity evaluation of various flexible resources has been widely studied. The concept of flexibility in power systems was proposed early. Degefa et al. [11] and Liu et al. [12] explain the concept of flexibility and propose a method for classifying the characteristics of flexible resources. Wen et al. [13] built a mathematical model of a unified energy storage form of flexible resources and calculated a high-precision cluster flexibility external model. Das et al. [14] propose the strategy of electric vehicle aggregation charging and evaluate the charging control method of electric vehicle aggregation. The electricity market is studied by considering the participation role of electric vehicle aggregators and individuals. Wang et al. [15] propose a coordinated evaluation method for aggregating electric vehicles without compromising the use by independent electric vehicle owners and for determining the flexibility of the optimal utilization time of electric vehicles after aggregation. Wang et al. [16] propose a virtual power-plant model containing a virtual generator and a virtual battery and present a high-dimensional polytope-based bound shrinking method to solve the whole feasible domain. Zhou et al. [17] aggregate electric vehicles as a controllable storage system via the Internet of Things, and a dispatchable region formation approach of electric vehicle aggregation is proposed to capture its available flexibility in the electricity market. Li et al. [18] consider the multi-demand response plan and the peak-filling effect of electric load, thermal load, and gas load aggregation, proposing a robust optimization model based on a data-driven set to improve the stability and economy of the system. Zhao et al. [19] aggregate distributed energy resources into a virtual power plant to participate in the wholesale market as a single entity. Pan et al. [20] construct a district heating system (DHS) model considering the thermal inertia of buildings and propose a greedy method for solving a new modified feasible domain by calculating a series of linear programming problems. However, the above research on the adjustable ability of IESs seldom investigates the coupling of multi-energy forms. With the rapid development of IESs for supplying multi-energy end-user loads, it is necessary for the UESS to understand the adjustable capability of the IES's effective incentive measures formulated to promote IES coordinate with the UESS.

In addition, economic concerns have been rarely mentioned in the above studies on adjustable capacity evaluation. Regarding economics, existing research mostly focuses on the optimal scheduling of IESs with the objective of the lowest operating cost or the highest profit. Somma et al. [21] optimize the operation of a distributed energy system (DES) and improve the overall power generation efficiency. Teng et al. [22] introduce a hybrid energy storage model based on electricity, hydrogen, thermal energy conversion, and energy storage, and propose a micro-grid autonomous operation strategy. Rahimi et al. [23] establish a dispatching model for a virtual power plant that satisfies both electrical and thermal loads to maximize the profit of participants. Wang et al. [24], based on modeling of an electric–thermal–natural gas network, propose an economic dispatching model of regional integrated energy systems. Xiang et al. [25] establish a comprehensive operation model of an electric–heat–natural gas coupling system with the goal of minimizing the economic cost considering the price-based and incentive-based demand response. Guo et al. [26] optimize data centers' energy generation and consumption, and their adjustable capacity potential is investigated. However, a specific operational strategy can only be obtained by the above research, which cannot reveal the adjustable capability of an IES when various economic constraints are considered. In practice, people do not strictly limit the operating cost to the minimum but consider setting it to be less than a certain value or controlling it within a certain interval when the regulating power is needed by the UESS's operator.

Meanwhile, in response to the carbon peaking by 2030 and carbon neutrality by 2060 proposed by China's government, CO_2 emissions should also be considered [27–29]. With the progress of various detection technologies, especially the intelligent and low-cost monitoring technology for different parameters such as temperature [30,31], the emissions of CO_2 can be well measured and promote the control of CO_2 further. Some researchers have investigated the impacts of carbon emission control on an IES's operation [32]. Wang et al. [33] develop a multi-objective optimization model considering system economy, system autonomy, and carbon emissions. Wang et al. [34] take into account the multiple uncertainties of renewable energy and propose a multi-objective optimal dispatching model that considers park-level participation in carbon market trading. However, the existing papers rarely focus on the impacts of carbon emissions on the evaluation of the adjustable capacity of an IES.

In this paper, to address the above problems, an IES is regarded and modeled as virtual energy storage for a UESS using a multi-objective optimization method for evaluating the parameters in the proposed virtual energy storage model of the IES. The coupling of multiple energy forms consisting of electricity, heat, and gas is considered in this work. The novelties and contributions of this paper are as follows:

(1) Considering the coupling of multiple types of energy forms in the IES and IES's interaction with upper-level energy supply systems, an aggregating model for demonstrating the adjustable capacity of the IES is proposed in this paper.
(2) Both demand response and economic constraints are involved in the proposed model, and a multi-objective optimization method is proposed to identify the relevant parameters in the proposed aggregating model.

The rest of this paper is organized as follows. The mathematical model of the IES is presented in Section 2. Section 3 proposes the economic costs of the IES including carbon emission costs. Section 4 defines the adjustable capacity of the IES and proposes the multi-objective model for identifying parameters. Section 5 carries out a case study, and Section 6 concludes this paper.

2. IES Modeling

2.1. Structure of the IES

The system structure of the integrated energy system is shown in Figure 1. The integrated energy system built in this paper includes three different energy forms as electricity, gas, and heat, which are composed of energy production equipment, energy conversion equipment, energy consumption equipment, and energy storage equipment [35–37]. Specifically, the selected equipment includes wind turbine (WT), photovoltaic (PV), electric boiler (EB), power-to-gas (P2G), combined heat and power (CHP), gas boiler (GB), electricity storage (ES), heat storage (HS), and gas storage (GS) units. The IES purchases and sells electricity and purchases gas for the upper-level distribution network and natural gas system. After the conversion of the coupling equipment, it is finally supplied to users in different energy forms. It should also be pointed out that the structure of the IES is proposed here to demonstrate the effectiveness of the presented adjustable capacity evaluation method. The presented method can be easily extended and applied for an IES with different energy equipment.

2.2. Mathematical Model

2.2.1. Renewable Energy

At any time, WT and PV have the maximum power related to wind speed, light intensity, temperature, and other factors, and this changes over time. In this paper, the maximum output of WT and PV in the next day is predicted based on the day-ahead phase, such as $P_{\mathrm{PV},t,\max}$ and $P_{\mathrm{W},t,\max}$.

$$\begin{cases} 0 \le P_{\mathrm{PV},t} \le P_{\mathrm{PV},t,\max} \\ 0 \le P_{\mathrm{W},t} \le P_{\mathrm{W},t,\max} \end{cases} \tag{1}$$

where $P_{PV,t}$ and $P_{W,t}$ are, respectively, the scheduled PV and WT power at time interval t. $P_{PV,t,max}$ and $P_{W,t,max}$ are, respectively, the maximum available power outputs of PV and WT at time interval t.

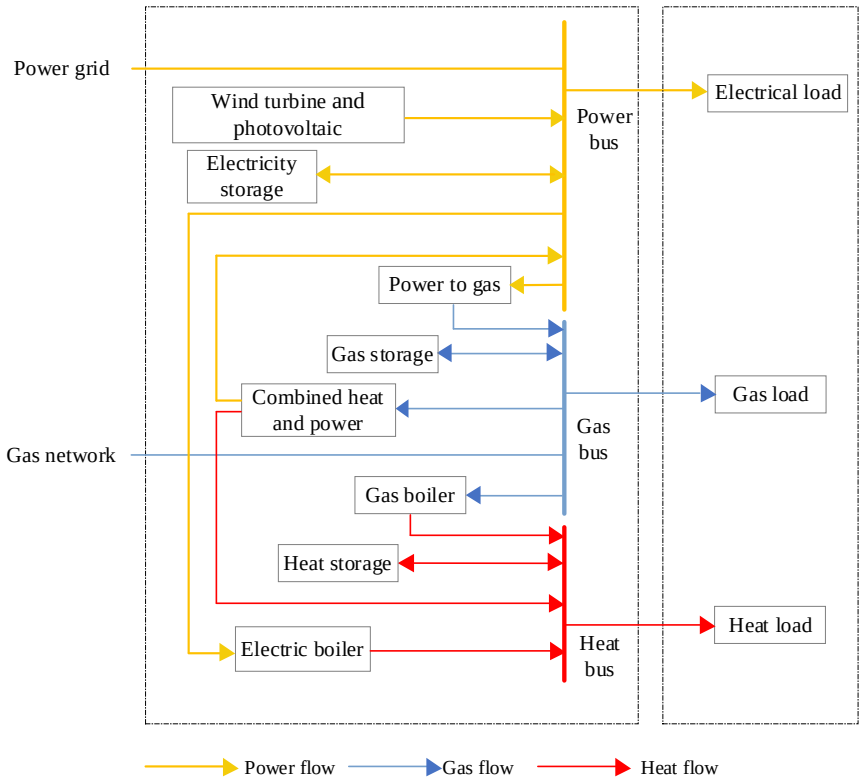

Figure 1. IES structure diagram.

2.2.2. Electric Boiler and Gas Boiler

An EB is an energy conversion device that converts electrical energy into heat energy, thereby supplying heat load. Its mathematical model and constraints in the operational process are as follows:

$$\begin{cases} H_{EB,t} = \eta_{EB} P_{EB,t} \\ 0 \le P_{EB,t} \le P_{EB,max} \end{cases} \quad (2)$$

where $H_{EB,t}$ is the heat production power of the EB at time interval t; η_{EB} is the heat production efficiency of the EB; $P_{EB,t}$ and $P_{EB,max}$ are, respectively, the consumed and maximum electric power of the EB at time interval t.

A GB is an energy-coupling device that converts the chemical energy in natural gas into heat energy by combustion to meet the thermal needs of users. The constraints of its operation are as follows:

$$\begin{cases} H_{GB,t} = G_{GB,t} \eta_{GB} \\ 0 \le H_{GB,t} \le H_{GB,max} \end{cases} \quad (3)$$

where $H_{GB,t}$ is the heat production power of the GB at time interval t; $G_{GB,t}$ is the natural gas power consumed by the GB at time interval t; η_{GB} is the heat production efficiency of the GB; and $H_{GB,max}$ is the maximum heat production power of the GB.

2.2.3. CHP System

CHP is a very important piece of equipment in the energy-coupling system. By burning natural gas, the chemical energy in natural gas is converted into electrical energy and thermal energy. Generally speaking, the operation mode of CHP is determined by heat and determined by electricity. The electricity and heat production of CHP under these two

operation modes are diverse. An IES can adjust its demand for energy by adjusting the operation mode [38]. The constraints of the CHP operational process are as follows:

$$\begin{cases} P_{\mathrm{CHP,min}} \le P_{\mathrm{CHP},t} \le P_{\mathrm{CHP,max}} \\ P_{\mathrm{CHP},t} = \mu_{\mathrm{CHP,P}} G_{\mathrm{CHP},t} \\ H_{\mathrm{CHP},t} = \mu_{\mathrm{CHP,H}} G_{\mathrm{CHP},t} \\ R_{\mathrm{CHP,down}} \le P_{\mathrm{CHP,t}} - P_{\mathrm{CHP,t-1}} \le R_{\mathrm{CHP,up}} \end{cases} \tag{4}$$

where $P_{\mathrm{CHP},t}$ and $H_{\mathrm{CHP},t}$ are, respectively, the electric and heat power of CHP at time interval t; $P_{\mathrm{CHP,max}}$ and $P_{\mathrm{CHP,min}}$ are the maximum and minimum electric powers of the unit, respectively; $G_{\mathrm{CHP},t}$ is the gas consumption of CHP at time interval t; $\mu_{\mathrm{CHP,P}}$ and $\mu_{\mathrm{CHP,H}}$ are the generation and heating efficiencies of CHP, respectively; and $R_{\mathrm{CHP,up}}$ and $R_{\mathrm{CHP,down}}$ the upward and downward ramping powers of CHP, respectively.

2.2.4. P2G Device

A P2G device can convert the additional electric energy generated by wind power, photovoltaic energy, or electric energy that cannot be consumed into artificial natural gas for storage. It is used during the valley load period. The main process of P2G technology is to first produce oxygen and hydrogen via electrolysis of water, and then hydrogen reacts with carbon dioxide to form methane gas.

The constraints of the P2G operation are as follows:

$$G_{\mathrm{P2G},t} = \eta_{\mathrm{P2G}} P_{\mathrm{P2G},t} \tag{5}$$

$$0 \le P_{\mathrm{P2G},t} \le P_{\mathrm{P2G,max}} \tag{6}$$

where $G_{\mathrm{P2G},t}$ is the power converted into artificial natural gas at time interval t; $P_{\mathrm{P2G},t}$ is the power consumed by P2G at time interval t; η_{P2G} is the conversion efficiency; $P_{\mathrm{P2G,max}}$ is the maximum electric power consumed by P2G.

2.2.5. Energy Storage Device

The different energy storage device model established in this paper includes power storage, heat storage, and gas storage devices. The operational principle of the three different energy forms of energy storage devices is similar, so one model can be used to describe the three energy storage devices. Here, using electric energy storage as an example, the mathematical model is as follows:

$$W_{\mathrm{es},t} = W_{\mathrm{es},t-1} + P_{\mathrm{esc},t}\gamma_{\mathrm{c}}\Delta t - \frac{P_{\mathrm{esd},t}}{\gamma_{\mathrm{d}}}\Delta t \tag{7}$$

where $W_{\mathrm{es},t}$ is the storage electricity of electric energy storage at time interval t.

Its capacity should have the following constraints:

$$W_{\mathrm{es,min}} \le W_{\mathrm{es},t} \le W_{\mathrm{es,max}} \tag{8}$$

where $W_{\mathrm{es,min}}$ and $W_{\mathrm{es,max}}$ are, respectively, the minimum and maximum storage capacities of electric energy storage.

The charge and discharge power of the energy storage device is continuously adjustable, but within a certain range, and the charging and discharging energies cannot be carried out at the same time, so the following constraints should be met:

$$\begin{cases} 0 \le P_{\mathrm{esc},t} \le B_{\mathrm{c},t} P_{\mathrm{esc,max}} \\ 0 \le P_{\mathrm{esd},t} \le B_{\mathrm{d},t} P_{\mathrm{esd,max}} \\ B_{\mathrm{c},t} + B_{\mathrm{d},t} \le 1 \end{cases} \tag{9}$$

where γ_c and γ_d are the charging and discharging efficiencies of electric energy storage, respectively; $P_{esc,t}$ and $P_{esd,t}$ are the charging and discharging powers of electric energy storage at time interval t, respectively; $P_{esc,max}$ and $P_{esd,max}$ are the maximum permitted charging and discharging powers of electric energy storage, respectively; $B_{c,t}$ and $B_{d,t}$ are binary variables indicating online and offline statuses of charging and discharging at time interval t, respectively.

In a scheduling period, the energy charged by the energy storage device should be equal to the energy released. At the beginning and end of a scheduling period, the stored energy should be equal, that is:

$$W_{es,0} = W_{es,T} \tag{10}$$

where $W_{es,0}$ and $W_{es,T}$ are the storage capacities at the beginning and end of the dispatch horizon, respectively.

2.3. Demand Respond

Demand response (DR) refers to users that adjust their energy-use behavior according to incentive mechanisms or electricity price, take part in grid interaction, optimize load curve, promote the uptake of renewable energy, and improve system operation efficiency [39]. According to the scheduling method, DR is divided into incentive-based demand response (IDR) [40] and price-based demand response (PDR) [41].

The load type can be divided into (1) basic loads: a fixed uncontrollable load in which the energy-use mode and energy-use time will not change; (2) shiftable loads: the running time of this kind of load can change with the plan, but it should be translated as a whole; (3) transferable loads: the power consumption time and power consumption can be flexibly changed, but in the whole scheduling horizon, it is necessary to meet the total load before and after the transfer to remain unchanged; (4) reducible loads: this kind of load can interrupt operation or reduce the running time and power consumption, and can be partially or completely reduced according to the actual situation.

The operation of shiftable loads and transferable loads can be changed, but there are some differences between them: When the demand response of a shiftable load occurs, it needs to be translated as a whole and the operation cannot be interrupted during operation and the power consumed cannot be changed, such as for a washing machine. When a transferable load participates in demand response, it does not need to shift the load. The power consumption time and power consumption can be freely adjusted, and the operation can be interrupted. However, it is necessary to ensure that the total load demand before and after the transfer of the transferable load remains unchanged. Compared with the shiftable load, its demand response characteristics are more flexible. The power consumption time and power consumption can be freely changed, such as for electric vehicles and energy storage.

2.3.1. IDR Modeling

(1) Shiftable loads

The operational constraints of shiftable loads are as follows:

$$\sum_{t=1}^{T} \alpha_t = t_{con} \tag{11}$$

$$\sum_{t=t_{st}}^{t_{st}+t_{con}-1} \alpha_t \geq t_{con}(\alpha_t - \alpha_{t-1} - \ldots - \alpha_{t-t_{con}+1}) \tag{12}$$

where α_t denotes the levelling state of the levelling load at time interval t, $\alpha_t = 1$ denotes that the load is levelling, $\alpha_t = 0$ denotes that the load is not levelling, t_{st} denotes the starting moment, and t_{con} denotes the duration of operation of the levelling load. Formula (11) limits the total operating hours of the translatable load. Formula (12) ensures that shiftable loads are able to be shifted as a whole.

(2) Transferable loads

Users can transfer some transferable loads from the peak period of electricity consumption or the period of high electricity price to the period of low electricity consumption or the period of low electricity price. The power transfer constraints of transferable loads are as follows:

$$P_{\text{tran},t,\min} \le P_{\text{tran},t} \le P_{\text{tran},t,\max} \tag{13}$$

$$\sum_{t=1}^{T} P_{\text{tran},t} = 0 \tag{14}$$

where $P_{\text{tran},t}$ is the transferred load at time interval t; $P_{\text{tran},t,\min}$ and $P_{\text{tran},t,\max}$ denote the minimum and maximum values of transferable loads, respectively. Formula (13) is the constraint on the amount of transferable load, and Formula (14) indicates that the total amount of transferable load remains constant during a dispatch horizon.

(3) Reducible loads

Load curtailment will directly reduce the power consumption of users during the peak period, such as lighting and air conditioning loads. The marking δ indicates the curtailment status of a curtailable load at a given time, $\delta = 1$ indicates a situation in which curtailment of the load occurs, and $\delta = 0$ indicates that the load is not curtailed. The power of the load curtailment after participating in demand response is as follows:

$$\delta_t P_{\text{cut},t}^{\max} \le P_{\text{cut},t} \le \delta_t P_{\text{cut},t}^{\max} \tag{15}$$

The maximum number of cuts is constrained as follows:

$$\sum_{t=1}^{24} \delta_t \le N_{\max} \tag{16}$$

where $P_{\text{cut},t}^{\max}$ is the power that can be curtailed at time interval t; $P_{\text{cut},t}$ is the curtailed load at time interval t; $N_{\max}$ is the maximum number of load curtailments.

2.3.2. PDR Modeling

Power loads also respond to the electricity price variation. The price–demand elasticity matrix is used to describe PDR characteristics. The element at the t-th row and j-th column in the elasticity matrix can be expressed as follows:

$$e_{t,j} = \frac{\Delta P_{\text{L},t} / P_{\text{L},t}}{\Delta \rho_j / \rho_j} \tag{17}$$

The constraints of PDR can be shown as:

$$\Delta P_{\text{SL},t} = P_{\text{SL},t} \left(\sum_{j=1}^{24} e_{t,j} \frac{\Delta \rho_j}{\rho_j} \right) \tag{18}$$

$$\sum_{t=1}^{T} \Delta P_{\text{SL},t} = 0 \tag{19}$$

$$-\Delta P_{\text{SL},\max} \le \Delta P_{\text{SL},t} \le \Delta P_{\text{SL},\max} \tag{20}$$

where $\Delta P_{\text{L},t}$ and $P_{\text{L},t}$ are, respectively, the load change for demand response and initial load at time interval t; $\Delta \rho_j$ is the electricity price change at time interval j; ρ_j is the initial electricity price at time interval j; $P_{\text{SL},t}$ is the initial power load at time interval t; $\Delta P_{\text{SL},t}$ is the load change after demand response at time interval t; $\Delta P_{\text{SL},\max}$ is the maximum load change of a price-based demand response.

3. Economic Costs of an IES

An IES regulates the operation of inner devices to coordinate with power grids. The operation of an IES should be constrained by operational costs since both the power system's operational safety and IES's economy should be balanced. The operational cost of an IES includes the cost of energy purchase, wind and photovoltaic abandonment costs, degradation cost of energy storage, carbon emission cost, and demand response cost as shown in Equation (21).

$$C_{\text{total}} = C_{\text{buy}} + C_{\text{w,pv}} + C_{\text{sto}} + C_{\text{car}} + C_{\text{DR}} \tag{21}$$

where C_{buy}, $C_{\text{w,pv}}$, C_{sto}, C_{car}, and C_{DR} are, respectively, the energy purchase cost of the IES, renewable energy abandonment costs, degradation cost of energy storage, carbon emission cost, and the cost of demand response.

3.1. Energy Purchase Cost and Constraints

The cost of electricity purchase includes the cost of electricity and gas purchase as expressed in Equation (22).

$$C_{\text{buy}} = \sum_{t=1}^{24} \left(p_{\text{P},t} P_{\text{grid},t} + p_{\text{G},t} G_{\text{buy},t} \right) \tag{22}$$

where $p_{\text{P},t}$ and $p_{\text{G},t}$ are prices of exchange electricity and gas at time interval t, respectively.

3.2. Wind and Photovoltaic Abandonment Costs

When renewable energy cannot be fully consumed, the abandoned renewable energy power causes abandonment costs as expressed in Equation (23).

$$C_{\text{w,pv}} = \alpha_{\text{w}} \sum_{t=1}^{24} \left(P_{\text{W},t,\max} - P_{\text{W},t} \right) + \alpha_{\text{pv}} \sum_{t=1}^{24} \left(P_{\text{PV},t,\max} - P_{\text{PV},t} \right) \tag{23}$$

where α_{w} and α_{pv} are the cost coefficients of wind and photovoltaic abandonment, respectively.

3.3. Degradation Cost of Energy Storage

The IES built in this paper includes an electric storage device, gas storage device, and heat storage device. Using electric storage as an example, the degradation cost of electric storage is expressed in Equation (24). Due to similar operational characteristics, the depreciation costs of gas and heat storage devices can be established by analogy with Equation (24).

$$C_{\text{sto}} = \sum_{t=1}^{24} \left(k_{\text{esc}} P_{\text{esc},t} + k_{\text{esd}} P_{\text{esd},t} \right) \tag{24}$$

where k_{esc} and k_{esd} are, respectively, the cost coefficients of charging and discharging.

3.4. Carbon Emission Cost

At present, China's electric power industry allocates the initial carbon emission quota in the form of gratuities. If the carbon emissions of an IES in actual operation are greater than the initial carbon emission quota, there will be extra carbon emission costs. This paper adopts the stepped trading carbon prices to establish the carbon emission model, and the more carbon emissions generated by the IES, correspondingly more carbon emission costs will be charged. The model of carbon emission cost is shown in Equations (25) and (26).

$$E_{\text{all}} = \sum_{t=1}^{24} \left(\mu_{\text{e}} P_{\text{grid},t} + \mu_{\text{g}} G_{\text{grid},t} - \mu_{\text{P2G}} G_{\text{P2G},t} \right) - E_{\text{IES}} \tag{25}$$

$$C_{\text{car}} = \begin{cases} \mu E_{\text{all}} & E_{\text{all}} \le l \\ \mu(1+\alpha)(E_{\text{all}} - l) + \mu l & l \le E_{\text{all}} \le 2l \\ \mu(1+2\alpha)(E_{\text{all}} - 2l) + \mu(2+\alpha)l & 2l \le E_{\text{all}} \le 3l \\ \mu(1+3\alpha)(E_{\text{all}} - 3l) + \mu(3+3\alpha)l & 3l \le E_{\text{all}} \le 4l \\ \mu(1+4\alpha)(E_{\text{all}} - 4l) + \mu(4+6\alpha)l & E_{\text{all}} \ge 4l \end{cases} \tag{26}$$

where μ is the cost per unit of carbon emissions; l is the length of the carbon emission interval; E_{all} is the total carbon emissions; E_{IES} is the free carbon credits of the IES; μ_{e} and μ_{g} are the carbon emission factors of electricity and gas purchases, respectively; μ_{P2G} is the carbon absorption factor of P2G.

3.5. Demand Response Cost

Since loads with IDR adjust their own energy-use behavior according to the instructions issued by the system operator, the demand response cost is paid to users for compensation. In this paper, we consider the IDR to include electric loads and thermal loads. Modeling the compensation cost of the demand response using electricity load as an example, the total cost of demand response compensation is shown in Equation (27).

$$C_{\text{DR}} = k_{\text{shift}} \sum_{t=1}^{24} P_{\text{shift},t} + k_{\text{tran}} \sum_{t=1}^{24} P_{\text{tran},t} + k_{\text{cut}} \sum_{t=1}^{24} P_{\text{cut},t} \tag{27}$$

where k_{shift}, k_{tran}, and k_{cut} are, respectively, the compensation prices for shiftable, transferable, and reducible loads.

4. Adjustable Capacity Evaluation Model for an IES

Because of the intricate coupling of multi-energy flows in an IES, its energy demand for the UESS which includes upper-level distribution grids and natural gas pipeline systems in this paper is an intricate and integrated load. The IES interacts with the UESS by purchasing and selling energy, such as electricity and natural gas. Meanwhile, the terminal load needs to be satisfied via energy production, conversion, and storage devices. Due to multi-energy coupling and demand response, the exchange electric and gas power of the IES with the UESS can be adjusted. The adjustable capability of the IES is defined as its potential to coordinate with the UESS while meeting its own multi-energy loads, expressed as Equations (28)–(33).

$$P_{\text{grid},t}^{\min} \le P_{\text{grid},t} \le P_{\text{grid},t}^{\max} \tag{28}$$

$$E_{\text{grid},t}^{\text{P,min}} \le \sum_{\tau=1}^{t} P_{\text{grid},\tau} \le E_{\text{grid},t}^{\text{P,max}} \tag{29}$$

$$G_{\text{grid},t}^{\min} \le G_{\text{grid},t} \le G_{\text{grid},t}^{\max} \tag{30}$$

$$E_{\text{grid},t}^{\text{G,min}} \le \sum_{\tau=1}^{t} G_{\text{grid},\tau} \le E_{\text{grid},t}^{\text{G,max}} \tag{31}$$

$$\begin{cases} F_{t,\min}(P_{\text{grid},t}^{\min}, G_{\text{grid},t}^{\min}) = 0 \\ F_{t,\max}(P_{\text{grid},t}^{\max}, G_{\text{grid},t}^{\max}) = 0 \end{cases} \tag{32}$$

$$\begin{cases} H_{t,\min}(E_{\text{grid},t}^{\text{P,min}}, E_{\text{grid},t}^{\text{G,min}}) = 0 \\ H_{t,\max}(E_{\text{grid},t}^{\text{P,max}}, E_{\text{grid},t}^{\text{G,max}}) = 0 \end{cases} \tag{33}$$

where $P_{\text{grid},t}^{\min}$ and $P_{\text{grid},t}^{\max}$ are, respectively, the minimum and maximum exchange electric powers of the IES with upper-level distribution grids at time interval t; $G_{\text{grid},t}^{\min}$ and $G_{\text{grid},t}^{\max}$ are,

respectively, the minimum and maximum exchange gas powers of the IES with upper-level natural gas systems at time interval t; $E^{\mathrm{P,min}}_{\mathrm{grid},t}$ and $E^{\mathrm{P,max}}_{\mathrm{grid},t}$ are the minimum and maximum accumulated electric powers in tie-lines between the IES and upper-level distribution grids at time interval t; $E^{\mathrm{G,min}}_{\mathrm{grid},t}$ and $E^{\mathrm{G,max}}_{\mathrm{grid},t}$ are the minimum and maximum accumulated gas powers in pipes between the IES and upper-level natural gas systems at time interval t; $F_t(\cdot)$ is the relationship of exchange of electric and gas power at time interval t; $H_t(\cdot)$ is the relationship of accumulated electric and gas power at time interval t.

Therefore, the adjustable capacity evaluation for the IES is to obtain parameters and coupling relations of exchange of electric and gas power of the IES with the UESS, as shown in Figure 2.

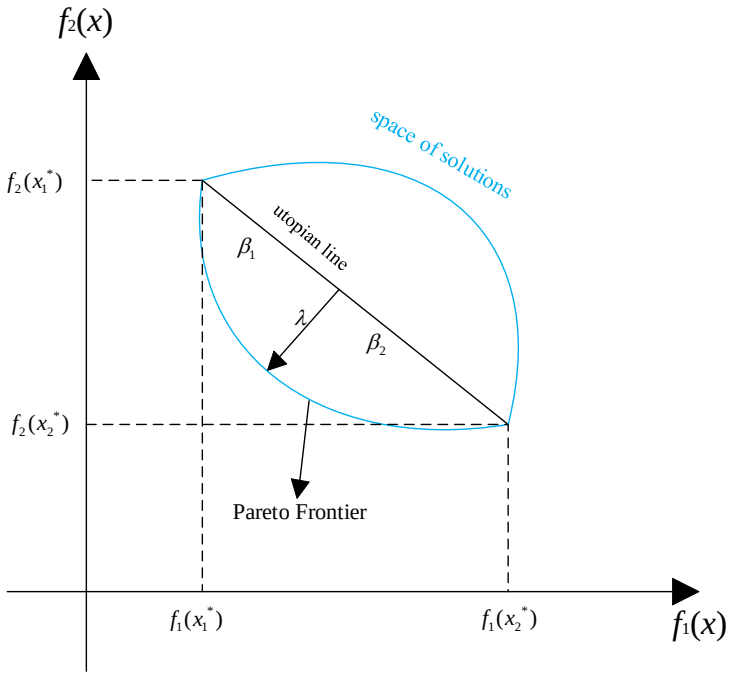

Figure 2. Schematic diagram of NBI algorithm for multi-objective problem.

4.1. Objective Function

As mentioned above, to obtain the parameters and relations in Equations (28)–(33), the following multi-objective optimization is established as shown in Equations (34)–(37). Equation (34) is used to identify $P^{\max}_{\mathrm{grid},t}$, $G^{\max}_{\mathrm{grid},t}$, and $F_{t,\max}(P^{\max}_{\mathrm{grid},t}, G^{\max}_{\mathrm{grid},t}) = 0$, while Equation (35) is used to identify $P^{\min}_{\mathrm{grid},t}$, $G^{\min}_{\mathrm{grid},t}$, and $F_{t,\min}(P^{\min}_{\mathrm{grid},t}, G^{\min}_{\mathrm{grid},t}) = 0$. Similarly, $E^{\mathrm{P,min}}_{\mathrm{grid},t}$, $E^{\mathrm{P,max}}_{\mathrm{grid},t}$, $E^{\mathrm{G,min}}_{\mathrm{grid},t}$, $E^{\mathrm{G,max}}_{\mathrm{grid},t}$, $H_{t,\min}(E^{\mathrm{P,min}}_{\mathrm{grid},t}, E^{\mathrm{G,min}}_{\mathrm{grid},t}) = 0$, and $H_{t,\max}(E^{\mathrm{P,max}}_{\mathrm{grid},t}, E^{\mathrm{G,max}}_{\mathrm{grid},t}) = 0$ can be identified using Equations (36) and (37).

$$\begin{cases} \max P_{\mathrm{grid},t} \\ \max G_{\mathrm{grid},t} \end{cases} \tag{34}$$

$$\begin{cases} \min P_{\mathrm{grid},t} \\ \min G_{\mathrm{grid},t} \end{cases} \tag{35}$$

$$\begin{cases} \max E^{\mathrm{P,max}}_{\mathrm{grid},t} \\ \max E^{\mathrm{G,max}}_{\mathrm{grid},t} \end{cases} \tag{36}$$

$$\begin{cases} \min E^{\mathrm{P,min}}_{\mathrm{grid},t} \\ \min E^{\mathrm{G,min}}_{\mathrm{grid},t} \end{cases} \tag{37}$$

4.2. Constraints

Despite the operational constraints of multiple devices as shown in Equations (1)–(20), during IES operation, the following constraints should be included:

(1) Power balance constraints

In the IES, a power balance of various forms of energy should be maintained during its operation.

$$P_{\text{grid},t} + P_{\text{PV},t,\text{c}} + P_{\text{w},t,\text{c}} + P_{\text{esd},t} + P_{\text{CHP},t} = P_{\text{P2G},t} + P_{\text{esc},t} + P_{\text{EB},t} + P_{\text{load},t} \tag{38}$$

$$G_{\text{grid},t} + G_{\text{P2G},t} + G_{\text{gd},t} = G_{\text{CHP},t} + G_{\text{GB},t} + G_{\text{gc},t} + G_{\text{load},t} \tag{39}$$

$$H_{\text{eb},t} + H_{\text{rd},t} + H_{\text{GB},t} + H_{\text{CHP},t} = H_{\text{rc},t} + H_{\text{load},t} \tag{40}$$

(2) Total cost constraint

$$C_{\text{total}} \leq \varepsilon C_{\text{total,min}} \tag{41}$$

where $C_{\text{total,min}}$ is the minimum operational cost of the IES, which can be obtained by solving the problem with the objective of minimizing C_{total}; ε is a pre-determined value that is larger than 1. Providing regulation power to upper-level distribution grids will change the operational strategy of the IES away from the most economic operation point, which correspondingly induces larger operational costs. ε indicates the tolerant maximum value of operational costs for the IES's operator.

4.3. NBI-Based Multi-Objective Solving

The adjustable capability evaluation model of the IES established in this paper is a multi-objective optimization problem, and the normal boundary intersection (NBI) method can be adopted. The NBI method is easy to realize by transforming the multi-objective problem into a single objective. For a multi-objective optimization problem as in Equation (42),

$$\begin{aligned} &\min F = \min[f_1(x), f_2(x)] \\ &s.t. \begin{cases} h(x) = 0 \\ g(x) \leq 0 \end{cases} \end{aligned} \tag{42}$$

f_1 and f_2 are objective functions; $h(x) = 0$ and $g(x) \leq 0$, respectively, denote equation and inequality constraints.

The specific process of the NBI algorithm is as follows:

(1) Solving for the optimal values of the two objective functions:

$$f_1({x_1}^*) = \min f_1(x), f_2({x_2}^*) = \min f_2(x)$$

Solve for $f_1({x_2}^*)$ and $f_2({x_1}^*)$ by substituting ${x_1}^*$ and ${x_2}^*$, respectively. By evaluating the matrix $\Phi = \begin{pmatrix} f_1({x_1}^*) & f_1({x_2}^*) \\ f_2({x_1}^*) & f_2({x_2}^*) \end{pmatrix}$ and connecting $(f_1({x_1}^*), f_2({x_1}^*))$ and $(f_1({x_2}^*), f_2({x_2}^*))$, the utopian line is obtained, as shown in Figure 2.

(2) Normalization: The solved objective function values are normalized and the normalized objective function is shown in Formula (43).

$$\begin{cases} \overline{f}_1(x) = \frac{f_1(x) - f_1({x_1}^*)}{f_1({x_2}^*) - f_1({x_1}^*)} \\ \overline{f}_2(x) = \frac{f_2(x) - f_2({x_2}^*)}{f_2({x_1}^*) - f_2({x_2}^*)} \end{cases} \tag{43}$$

The normalized matrix is: $\overline{\Phi} = \begin{pmatrix} 0 & 1 \\ 1 & 0 \end{pmatrix}$.

The distance λ between any point (β_1, β_2) on the utopian line and a point $(\overline{f}_1(x), \overline{f}_2(x))$ on the Pareto frontier is:

$$\begin{cases} \lambda = \beta_1 - f_1(x) \\ \lambda = \beta_2 - f_2(x) \end{cases} \tag{44}$$

where $\beta_1 + \beta_2 = 1$ and $0 \leq \beta_1, \beta_2 \leq 1$.

The normalized schematic is shown in Figure 3.

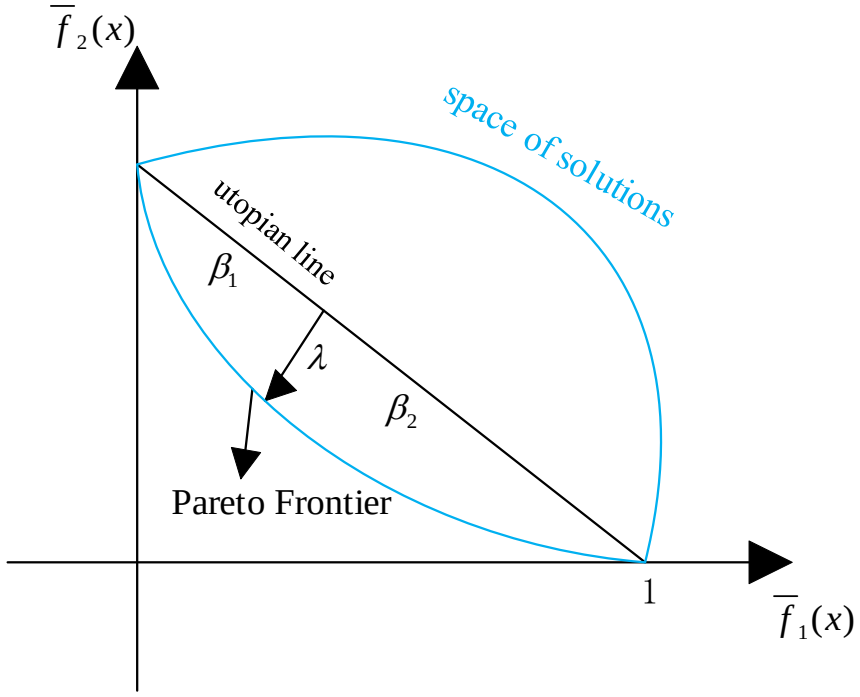

Figure 3. Schematic diagram of NBI algorithm after normalization.

(3) Solving single-objective optimization problems

The Pareto solution set in the multi-objective problem can be obtained by solving the maximized distance λ. We can change the values of β_1 and β_2 to keep distance moving and the Pareto frontier can be obtained. So, the original multi-objective problem can be transformed into a series of single-objective problems as in Equation (45).

$$\max \lambda \quad s.t. \begin{cases} \lambda = \beta_1 - f_1(x) \\ \lambda = \beta_2 - f_2(x) \\ \beta_1 + \beta_2 = 1 \end{cases} \tag{45}$$

5. Case Study

5.1. Basic Data

In this paper, an IES as shown in Figure 1 is selected for simulation to evaluate the adjustable capacity during a typical day. Renewable energy includes wind and photovoltaic power and their output curves are shown in Figure 4. The PV output is 0 at night, and the PV output is larger at time intervals 10 to 15, when sunlight is more abundant. The wind is lower at midday and higher at night, with more output from wind turbines at night and less output from wind turbines at midday. The load demand of the IES includes electric load, heat load, and gas load. Load demand curves are shown in Figure 5. The load demand is higher in the daytime and lower at night. The parameters of the energy-coupling devices and energy storage devices in the IES are shown in Tables 1 and 2. Demand response parameters are shown in Table 3. To demonstrate the effectiveness and feasibility of the proposed model, five scenarios are set with regards to whether demand response and

economic constraints are considered, as shown in Table 4. Based on the above scenarios, the adjustable capacity evaluation of the IES is solved and compared in this study.

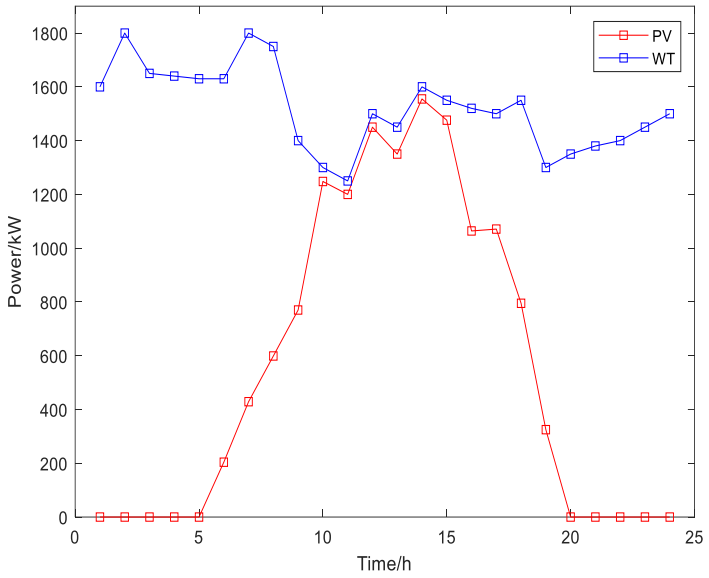

Figure 4. Output curves of wind power and photovoltaic power.

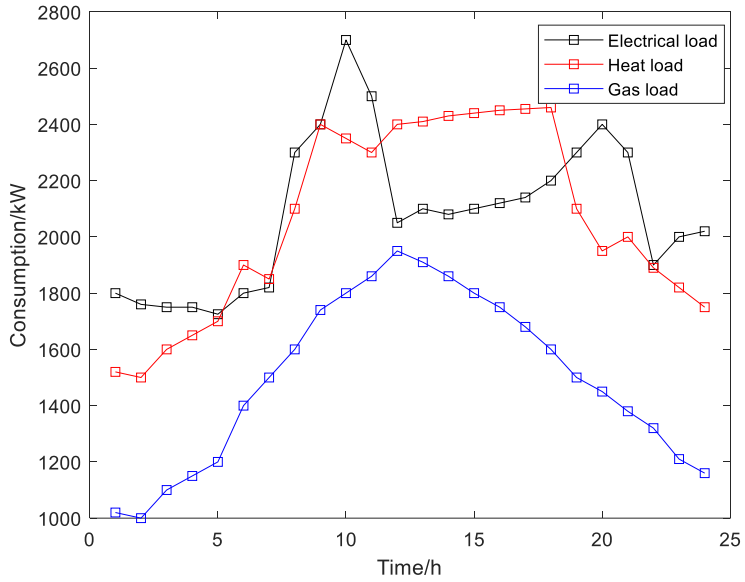

Figure 5. Load demand curves.

Table 1. Coupling device parameters.

Coupling Device	Maximum/Minimum Power	Conversion Efficiency	Rate of Climb
P2G	1000/0	0.85	
EB	500/0	0.85	
GB	1000/0	0.9	
CHP	Generating power: 1000/0	0.4	Uphill rate: 100
	Heating power: 1333.33/0	0.3	Downhill rate: −50

Table 2. Parameters of energy storage equipment.

Energy Storage Device	Maximum Reserves	Initial Reserves	Maximum Charge/Discharge Power	Charge/Discharge Efficiency
Storage battery	3000	500	250/250	0.98/0.98
Gas storage	3000	500	250/250	0.98/0.98
Heat storage	4000	0	1000/1000	0.95/0.9

Table 3. Demand response parameters.

Load Type	Continuous Runtime/h	Time Period of Operation	Power/kW	Compensation Price/CNY·kWh^{-1}
Shiftable electrical loads A	2	5:00–20:00	250	0.2
Shiftable electrical loads B	3	7:00–21:00	250	0.2
Shiftable heat loads	3	5:00–19:00	450	0.1
Transferable electrical loads	4	0:00–24:00	250	0.3
Load Type	Maximum number of reductions		Compensation price/CNY·kWh^{-1}	
Reducible electrical loads	8		0.4	
Reducible heat loads	8		0.2	

Table 4. Simulation scenarios.

Scenario	IDR	PDR	Economic Constraints
I	×	×	×
II	√	×	×
III	×	√	×
IV	√	×	√
V	×	√	√

5.2. Results Analysis

5.2.1. Adjustable Capacity in Scenario I

In scenario I, both the demand response and economic constraints are not considered, and the coupling relation of exchanged electric and gas power at the single-time interval 12 is shown in Figure 6a. The coupling relation of accumulated exchanged electric and gas power at single-time interval 12 is shown in Figure 6b. When considering the time dimension, the adjustable capacity of the IES is a three-dimensional surface, as shown in Figure 7. For the lower boundary of coupling relations of exchanged electric and gas power, the maximum exchanged electric power corresponds to the minimum exchanged natural gas power, and vice versa. Due to energy storage and renewable energy abandonment, the coupling relations of electric and natural gas power are not a line but interact within a certain range.

5.2.2. Influence of Demand Response on the Adjustable Capability of the IES

To illustrate the influence of demand response on the adjustable capacity of the IES, scenarios II and III are set to be compared with scenario I. The adjustable capacities of the IES in scenarios II and III are shown in Figures 8 and 9, respectively.

As shown in Figure 8, compared with scenario I, the adjustable capacity of the IES expands when the IDR is considered in scenario II. The upper boundary of coupling relations of exchanged electric and natural gas power is taken as an example to illustrate the reason. When the IDR is integrated into scenario II, the shiftable electric and thermal loads and the transferable electric load will all be shifted and transferred to a certain time interval, in response to the objective of maximizing electric and gas power exchange at the time interval. Also, at that time interval, the reducible load will not be reduced. At the same time, wind power and photovoltaic power are abandoned. Accordingly, in order to

minimize exchange power, the IES will fully absorb wind power and photovoltaic power, and all shiftable loads and transferable loads will be shifted and transferred away from the time interval, and reducible loads will be reduced.

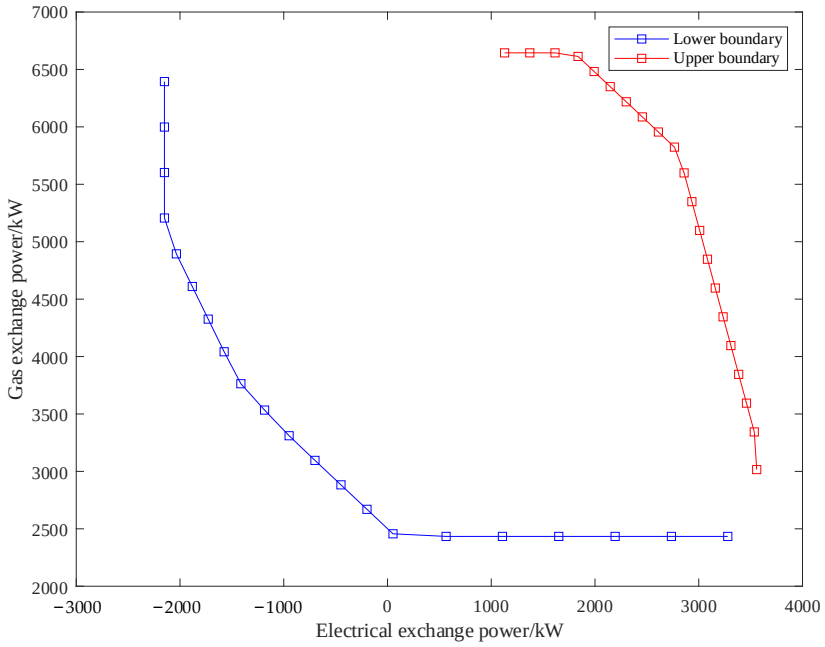

(**a**)

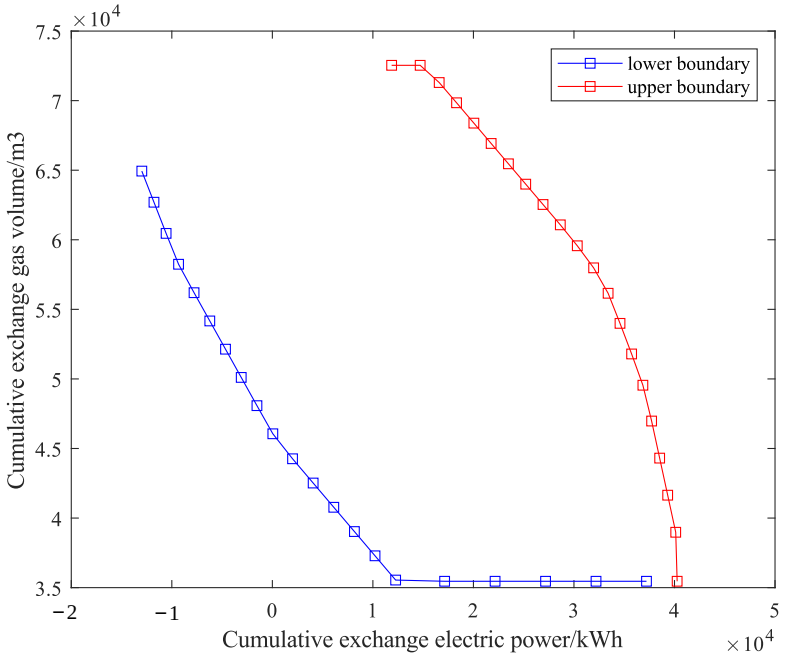

(**b**)

Figure 6. Adjustable capacity at a single time interval in scenario I. (**a**) coupling relation of exchanged electric and gas power; (**b**) coupling relation of accumulated exchanged electric and gas power.

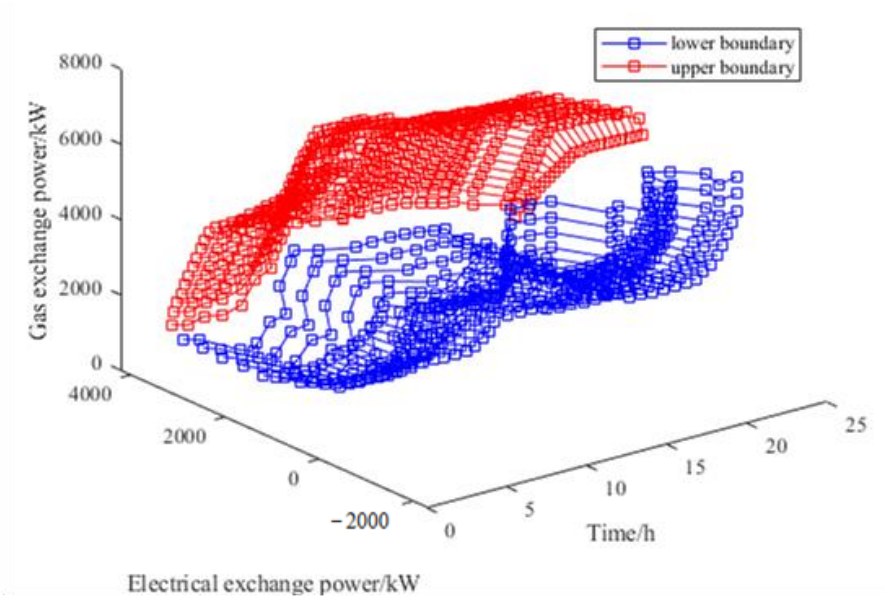

(**a**)

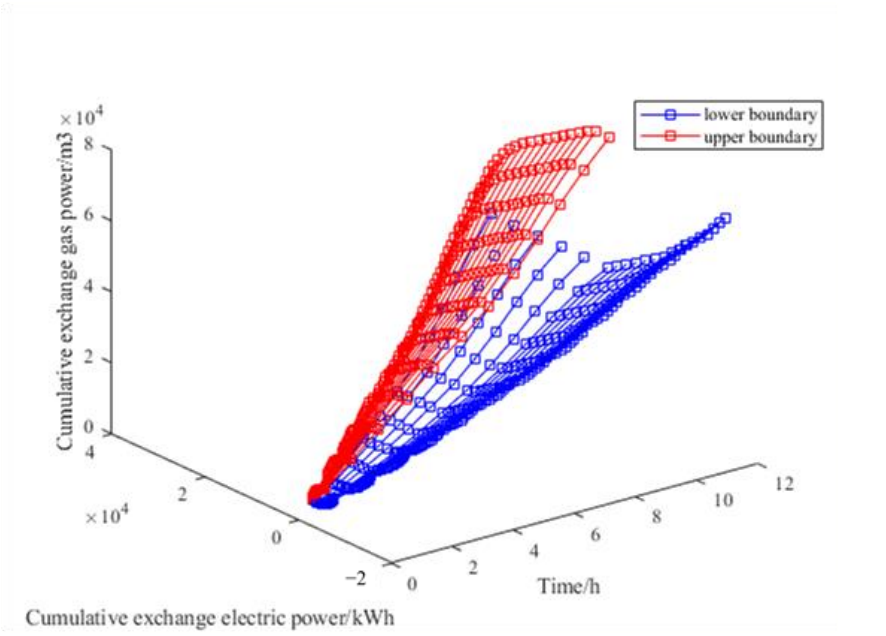

(**b**)

Figure 7. Three-dimensional adjustable capacity in scenario I. (**a**) coupling relation of exchanged electric and gas power; (**b**) coupling relation of accumulated exchanged electric and gas power.

As shown in Figure 9, the range of adjustable capacity of the IES will also expand after considering the PDR. When evaluating the maximum exchanged electric power at the 12-th time interval, the IES's operator will reduce the price of electricity. After the demand response occurs, the electric power load at the time interval increases and outputs of wind and photovoltaic power are curtailed. Correspondingly, the lower boundary of the adjustable capacity of the IES can be obtained by increasing the electricity price at this moment to reduce the energy consumption on the demand side. In summary, when demand response is considered, the range of the adjustable capacity of the IES will be expanded accordingly.

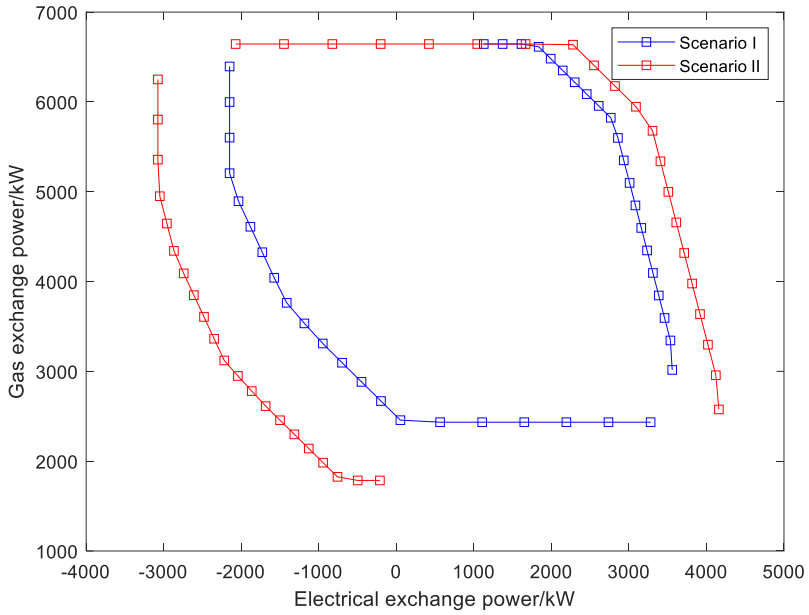

(**a**)

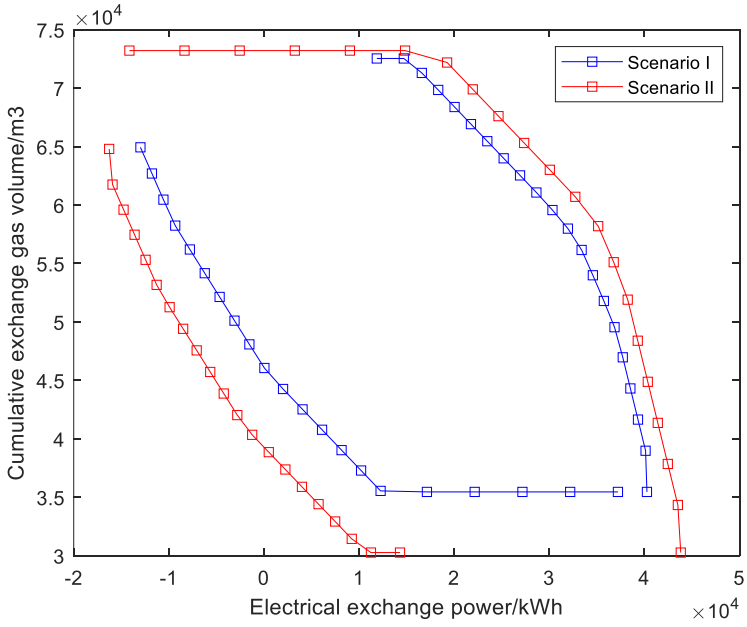

(**b**)

Figure 8. Comparison of adjustable capacities in scenario I and scenario II. (**a**) Coupling relations of exchanged electric and gas power; (**b**) Coupling relations of accumulated exchanged electric and gas power.

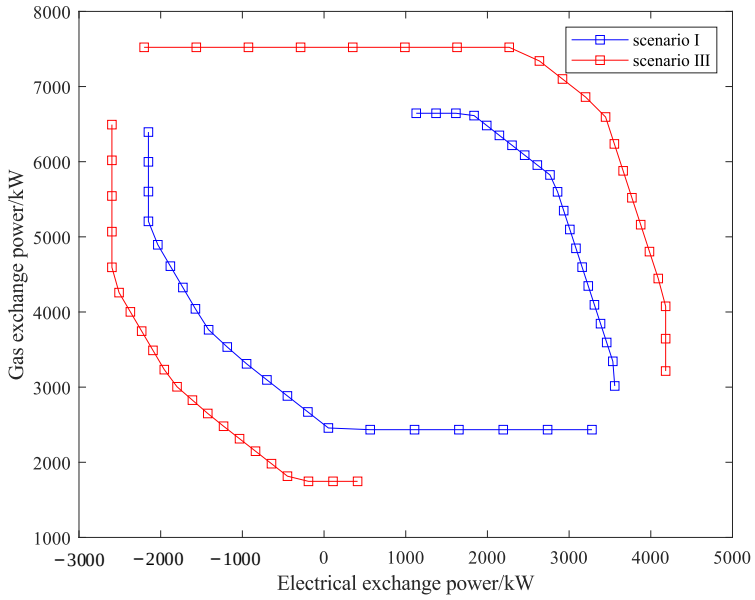

(**a**)

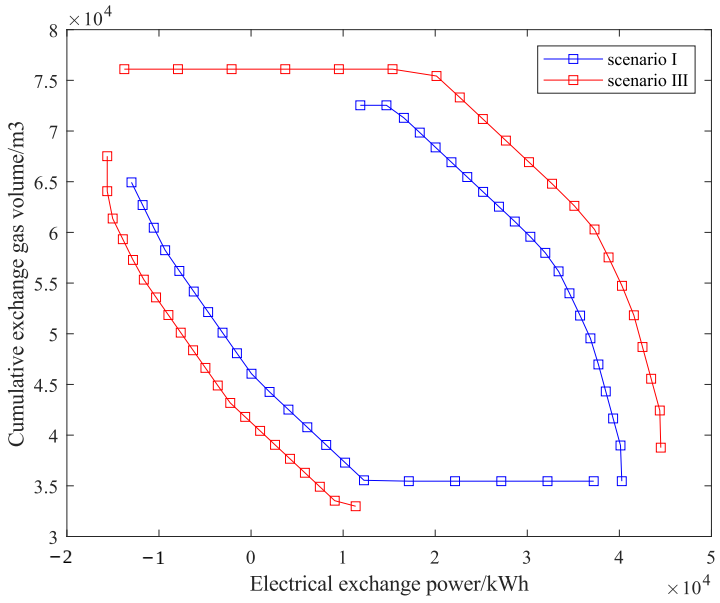

(**b**)

Figure 9. Comparison of adjustable capacities in scenario I and scenario III. (**a**) Coupling relations of exchanged electric and gas power; (**b**) Coupling relations of accumulated exchanged electric and gas power.

5.2.3. Influence of Economic Constraints on the Adjustable Capability of the IES

Economic constraints have a wider effect on the adjustable capacity evaluation of the IES. Economic constraints affect the all-operation period. The smaller the value of ε is, the narrower the adjustable capacity of the IES will be. In this case, lower-cost operational strategies are more inclined to be chosen by the IES. When ε equals 1, it means that the IES is constrained to the point with the smallest operational costs. Then, no adjustable capacity can be provided by the IES. Obviously, if there are too-tight total economic constraints, in a dispatching horizon, all operational strategies may not meet the extreme situational economic constraints. As shown in Figures 10 and 11, with economic constraints, the

adjustable capacity of the IES significantly narrows. In scenario IV, the IDR is a response mode that changes the load behavior via the command issued by upper-level distribution grids. Therefore, demand response compensation costs will further limit the range of adjustable capacity of the IES. In contrast, PDR enables users to spontaneously adjust their energy-use behavior by adjusting the energy-use price. There are no additional demand response compensation constraints, meaning there is more adjustable space in the purchase of energy, so the adjustable capacity range under scenario V is slightly larger than that under scenario IV.

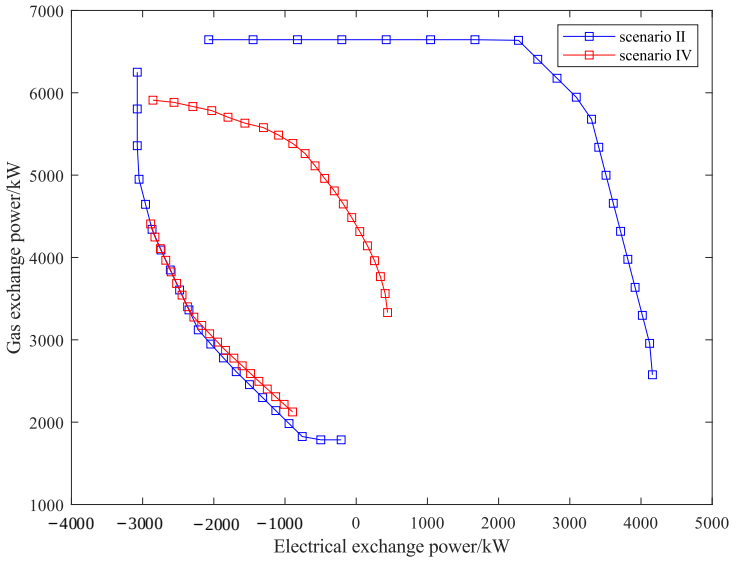

(**a**)

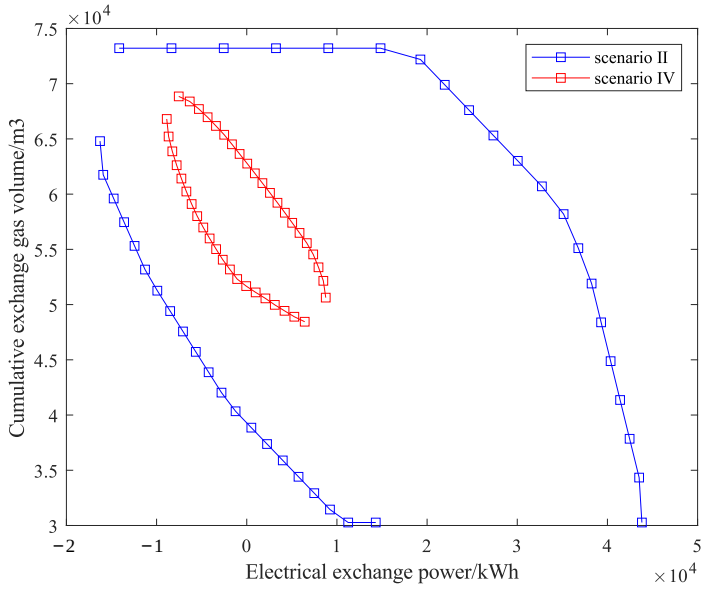

(**b**)

Figure 10. Comparison of adjustable capacities in scenario II and scenario IV. (**a**) Coupling relations of exchanged electric and gas power; (**b**) Coupling relations of accumulated exchanged electric and gas power.

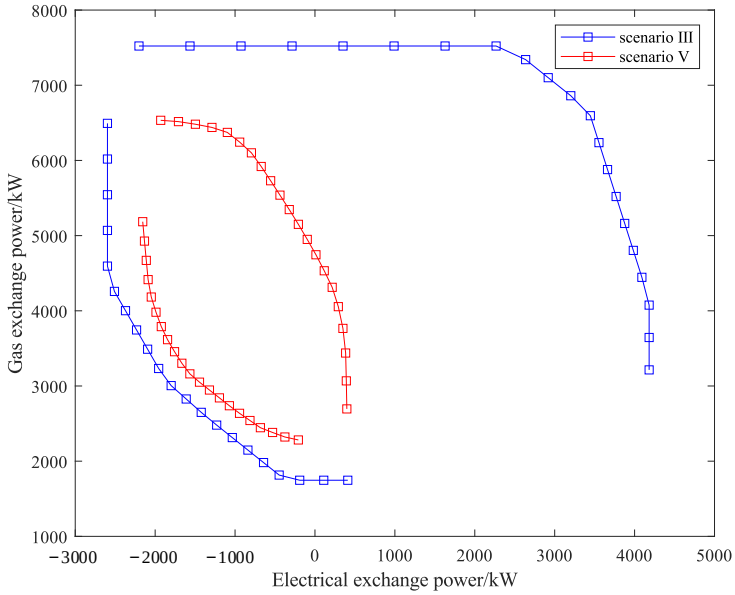

(**a**)

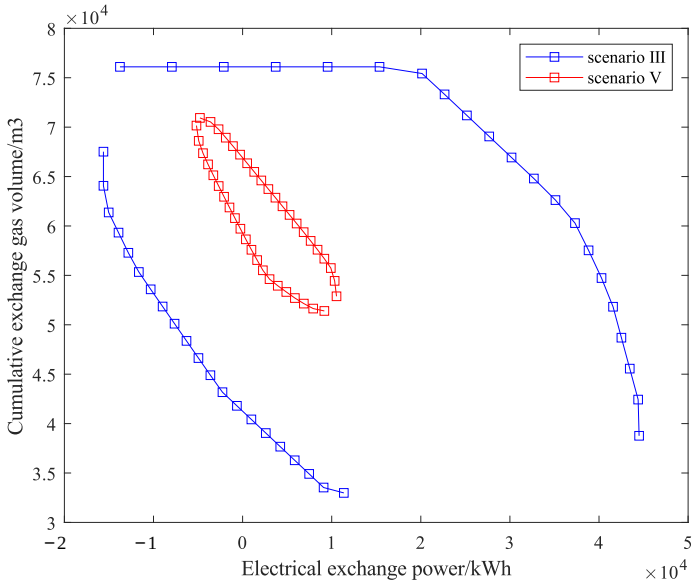

(**b**)

Figure 11. Comparison of adjustable capacities in scenario III and scenario IV. (**a**) Coupling relations of exchanged electric and gas power; (**b**) Coupling relations of accumulated exchanged electric and gas power.

6. Conclusions

This paper presents an NBI-based multi-objective optimization model for evaluating the adjustable capacity range of an IES. The effects of demand response and economic constraints on the adjustable capability of the IES are included. The effectiveness of the method was verified using simulation examples, and the following conclusions were drawn:

(1) The adjustable capacity of an IES can be modeled as virtual energy storage, which can be further applied into existing dispatching architecture. Many factors including renewable energy generation, multiple types of energy storage, and demand response can impact the adjustable capacity of an IES. Specifically, both energy storage and demand response can be adjusted to extend the adjustable capacity.

(2) Economic constraints limit the adjustable capacity of an IES by affecting the operation of a variety of equipment. The adjustable capacity is significantly reduced with economic constraints, which indicates that the regulation power provided by the IES to the UESS causes extra operational costs. The IES can adjust its adjustable capacity by changing the budget, which makes the IES more competitive in the market.
(3) Due to the energy conversion of multi-energy sectors, the electricity and natural gas demands of the IES for the UESS are deeply coupled. The electricity demand decreases while the natural gas demand increases, and the coupling relationship functions can be pictured using proposed multi-objective methods.

Various uncertainties including wind power, photovoltaic power, and demand will obviously impact the robustness and accuracy of the adjustable capacity evaluation of an IES, which is not studied in this paper. In addition, the multi-time-scale characteristics of the energy sectors of electricity, gas, and heat are not considered. In our future work, the influences of uncertainties and multi-time-scale characteristics on the adjustable capacity of IESs will be investigated. The optimal coordination of an IES with a UPSS will be studied as well.

Author Contributions: Conceptualization, Y.L. and R.L.; methodology, R.L.; software, R.L. and L.S.; validation, F.W. and J.Z.; formal analysis, J.L.; investigation, K.L.; resources, K.L.; data curation, L.S.; writing—original draft preparation, Y.L. and R.L.; writing—review and editing, L.S. and F.W.; visualization, J.Z.; supervision, Y.L.; project administration, Y.L. All authors have read and agreed to the published version of the manuscript.

Funding: This work was supported by the Natural Science Foundation of China under Grant 52107088; Natural Science Foundation of Jiangsu Province under Grant BK20210365; China Postdoctoral Science Foundation under Grant 2021M701039; and the Fundamental Research Funds for the Central Universities of China under Grant B200201019.

Data Availability Statement: Data is contained within the article.

Conflicts of Interest: Authors Jianhua Zhou and Jian Liu were employed by the company State Grid Jiangsu Electric Power Company Research Institute. The remaining authors declare that the research was conducted in the absence of any commercial or financial relationships that could be construed as a potential conflict of interest.

References

1. Wang, C.; Ju, P.; Lei, S.; Wang, Z.; Wu, F.; Hou, Y. Markov decision process-based resilience enhancement for distribution systems: An approximate dynamic programming approach. *IEEE Trans. Smart Grid* **2020**, *11*, 2498–2510. [CrossRef]
2. Zhang, Y.Q.; Zang, W.; Zheng, J.H.; Cappietti, L.; Zhang, J.S.; Zheng, Y.; Fernandez-Rodriguez, E. The influence of waves propagating with the current on the wake of a tidal stream turbine. *Appl. Energy* **2021**, *290*, 116729. [CrossRef]
3. Wang, C.; Hou, Y.; Qiu, F.; Lei, S.; Liu, K. Resilience enhancement with sequentially proactive operation strategies. *IEEE Trans. Power Syst.* **2017**, *32*, 2847–2857. [CrossRef]
4. Zhang, Y.Q.; Zhang, Z.; Zheng, J.H.; Zheng, Y.; Zhang, J.S.; Liu, Z.Q.; Fernandez-Rodriguez, E. Research of the array spacing effect on wake interaction of tidal stream turbines. *Ocean Eng.* **2023**, *276*, 114227. [CrossRef]
5. Wang, C.; Cui, B.; Wang, Z. Analysis of solvability boundary for droop-controlled microgrids. *IEEE Trans. Power Syst.* **2018**, *33*, 5799–5802. [CrossRef]
6. Pan, C.; Jin, T.; Li, N.; Wang, G.; Hou, X.; Gu, Y. Multi-objective and two-stage optimization study of integrated energy systems considering P2G and integrated demand responses. *Energy* **2023**, *270*, 126846. [CrossRef]
7. Fattahi, A.; Sijm, J.; Faaij, A. A systemic approach to analyze integrated energy system modeling tools: A review of national models. *Renew. Sustain. Energy Rev.* **2020**, *133*, 110195. [CrossRef] [PubMed]
8. Li, G.; Zhang, R.; Jiang, T.; Chen, H.; Bai, L.; Cui, H.; Li, X. Optimal dispatch strategy for integrated energy systems with CCHP and wind power. *Appl. Energy* **2017**, *192*, 408–419. [CrossRef]
9. Tan, Z.; Zhong, H.; Wang, J.; Xia, Q.; Kang, C. Enforcing intra-regional constraints in tie-line scheduling: A projection-based framework. *IEEE Trans. Power Syst.* **2019**, *34*, 4751–4761. [CrossRef]
10. Zhao, H.; Wang, B.; Pan, Z.; Sun, H.; Guo, Q.; Xue, Y. Aggregating additional flexibility from quick-start devices for multi-energy virtual power plants. *IEEE Trans. Sustain. Energy* **2020**, *12*, 646–658. [CrossRef]
11. Degefa, M.Z.; Sperstad, I.B.; Sæle, H. Comprehensive classifications and characterizations of power system flexibility resources. *Electr. Power Syst. Res.* **2021**, *194*, 107022. [CrossRef]

12. Liu, H.; Zhao, Y.; Gu, C.; Ge, S.; Yang, Z. Adjustable capability of the distributed energy system: Definition, framework, and evaluation model. *Energy* **2021**, *222*, 119674. [CrossRef]
13. Wen, Y.L.; Hu, Z.C.; You, S.; Duan, X. Aggregate feasible region of DERs: Exact formulation and approximate models. *IEEE Trans. Smart Grid* **2022**, *13*, 4405–4423. [CrossRef]
14. Das, H.S.; Rahman, M.M.; Li, S.; Tan, C.W. Electric vehicles standards, charging infrastructure, and impact on grid integration: A technological review. *Renew. Sustain. Energy Rev.* **2020**, *120*, 109618. [CrossRef]
15. Wang, L.; Kwon, J.; Schulz, N.; Zhou, Z. Evaluation of aggregated EV flexibility with TSO-DSO coordination. *IEEE Trans. Sustain. Energy* **2022**, *13*, 2304–2315. [CrossRef]
16. Wang, S.; Wu, W. Aggregate flexibility of virtual power plants with temporal coupling constraints. *IEEE Trans. Smart Grid* **2021**, *12*, 5043–5051. [CrossRef]
17. Zhou, M.; Wu, Z.; Wang, J.; Li, G. Forming dispatchable region of electric vehicle aggregation in microgrid bidding. *IEEE Trans. Ind. Inform.* **2021**, *17*, 4755–4765. [CrossRef]
18. Li, Y.; Zhang, F.; Li, Y.; Wang, Y. An improved two-stage robust optimization model for CCHP-P2G microgrid system considering multi-energy operation under wind power outputs uncertainties. *Energy* **2021**, *223*, 120048. [CrossRef]
19. Zhao, C.; Fan, L. A data-driven model of virtual power plants in day-ahead unit commitment. *IEEE Trans. Power Syst.* **2019**, *34*, 5125–5135.
20. Pan, Z.; Guo, Q.; Sun, H. Feasible region method based integrated heat and electricity dispatch considering building thermal inertia. *Appl. Energy* **2017**, *192*, 395–407. [CrossRef]
21. Somma, M.D.; Yan, B.; Bianco, N.; Graditi, G.; Luh, P.B.; Mongibello, L.; Naso, V. Operation optimization of a distributed energy system considering energy costs and exergy efficiency. *Energy Convers. Manag.* **2015**, *103*, 739–751. [CrossRef]
22. Teng, Y.; Sun, P.; Hui, Q.; Chen, Z. A model of electro-thermal hybrid energy storage system for autonomous control capability enhancement of multi-energy microgrid. *CSEE J. Power Energy Syst.* **2019**, *5*, 489–497.
23. Rahimi, M.; Ardakani, F.J.; Ardakani, A.J. Optimal stochastic scheduling of electrical and thermal renewable and nonrenewable resources in virtual power plant. *Int. J. Electr. Power Energy Syst.* **2021**, *127*, 106658. [CrossRef]
24. Wang, Y.; Wang, Y.; Huang, Y.; Yang, J.; Ma, Y.; Yu, H.; Zeng, M.; Zhang, F.; Zhang, Y. Operation optimization of regional integrated energy system based on the modeling of electricity-thermal-natural gas network. *Appl. Energy* **2019**, *251*, 113410. [CrossRef]
25. Xiang, Y.; Cai, H.; Gu, C.; Shen, X. Cost-benefit analysis of integrated energy system planning considering demand response. *Energy* **2020**, *192*, 116632. [CrossRef]
26. Guo, C.; Luo, F.; Cai, Z.; Dong, Z.Y. Integrated energy systems of data centers and smart grids: State-of-the-art and future opportunities. *Appl. Energy* **2021**, *301*, 117474. [CrossRef]
27. Yun, Y.; Zhang, D.; Yang, S.; Li, Y.; Yan, J. Low-carbon optimal dispatch of integrated energy system considering the operation of oxyfuel combustion coupled with power-to-gas and hydrogen doped gas equipment. *Energy* **2023**, *283*, 129127. [CrossRef]
28. Sun, Q.; Wang, X.; Liu, Z.; Mirsaeidi, S.; He, J.; Wei, P. Multi-agent energy management optimization for integrated energy systems under the energy and carbon co-trading market. *Appl. Energy* **2022**, *324*, 119646. [CrossRef]
29. Wang, R.; Wen, X.; Wang, X.; Fu, Y.; Zhang, Y. Low carbon optimal operation of integrated energy system based on carbon capture technology, LCA carbon emissions and ladder-type carbon trading. *Appl. Energy* **2022**, *3*, 118664. [CrossRef]
30. Mobaraki, B.; Pascual, F.J.C.; Lozano-Galant, F.; Lozano-Galant, J.A.; Soriano, R.P. In situ U-value measurement of building envelopes through continuous low-cost monitoring. *Case Stud. Therm. Eng.* **2023**, *43*, 102778. [CrossRef]
31. Mobaraki, B.; Pascual, F.J.C.; Garcia, A.M.; Mascaraque, M.Á.M.; Vázquez, B.F.; Alonso, C. Studying the impacts of test condition and nonoptimal positioning of the sensors on the accuracy of the in-situ U-value measurement. *Heliyon* **2023**, *9*, e17282. [CrossRef] [PubMed]
32. Sun, P.; Hao, X.; Wang, J.; Shen, D.; Tian, L. Low-carbon economic operation for integrated energy system considering carbon trading mechanism. *Energy Sci. Eng.* **2021**, *9*, 2064–2078. [CrossRef]
33. Wang, Y.; Wang, X.; Yu, H.; Huang, Y.; Dong, H.; Qi, C.; Baptiste, N. Optimal design of integrated energy system considering economics, autonomy and carbon emissions. *J. Clean. Prod.* **2019**, *225*, 563–578. [CrossRef]
34. Wang, L.; Dong, H.; Lin, J.; Zeng, M. Multi-objective optimal scheduling model with IGDT method of integrated energy system considering ladder-type carbon trading mechanism. *Int. J. Electr. Power Energy Syst.* **2022**, *143*, 108386. [CrossRef]
35. Bischi, A.; Taccari, L.; Martelli, E.; Amaldi, E.; Manzolini, G.; Silva, P.; Campanari, S.; Macchi, E. A detailed MILP optimization model for combined cooling, heat and power system operation planning. *Energy* **2014**, *74*, 12–26. [CrossRef]
36. Wang, Y.; Cai, C.; Liu, C.; Han, X.; Zhou, M. Planning research on rural integrated energy system based on coupled utilization of biomass-solar energy resources. *Sustain. Energy Technol. Asses.* **2022**, *53*, 102416. [CrossRef]
37. Zhou, Y.; Min, C.; Wang, K.; Xie, L.; Fan, Y. Optimization of integrated energy systems considering seasonal thermal energy storage. *J. Energy Storage* **2023**, *71*, 108094. [CrossRef]
38. Mago, P.J.; Fumo, N.; Chamra, L.M. Performance analysis of CCHP and CHP systems operating following the thermal and electric load. *Int. J. Energy Res.* **2009**, *33*, 852–864. [CrossRef]
39. Huang, W.; Zhang, N.; Kang, C.; Li, M.; Huo, M. From demand response to integrated demand response: Review and prospect of research and application. *Prot. Control Mod. Power Syst.* **2019**, *4*, 12. [CrossRef]

40. Jiang, Y.; Xu, J.; Sun, Y.; Wei, C.; Wang, J.; Ke, D.; Li, X.; Yang, J.; Peng, X.; Tang, B. Day-ahead stochastic economic dispatch of wind integrated power system considering demand response of residential hybrid energy system. *Appl. Energy* **2017**, *190*, 1126–1137. [CrossRef]
41. Behboodi, S.; Chassin, D.P.; Crawford, C.; Djilali, N. Renewable resources portfolio optimization in the presence of demand response. *Appl. Energy* **2016**, *162*, 139–148. [CrossRef]